Nonlinear behavior for the uniform mode and horizontal standing spin-wave modes in metallic ferromagnetic microstrips: Experiment and theory

M. P. Wismayer, B.W. Southern, X. L. Fan, Y. S. Gui, C.-M. Hu, and R. E. Camley

Phys. Rev. B **85**, 064411 — Published 21 February 2012

DOI: 10.1103/PhysRevB.85.064411

Nonlinear Behavior for the Uniform Mode and Horizontal Standing Spin Wave Modes in Metallic Ferromagnetic Microstrips: Experiment and Theory

M.P. Wismayer, B.W. Southern, X. L. Fan, Y.S. Gui, C.-M. Hu

Department of Physics and Astronomy,

University of Manitoba, Winnipeg, Canada R3T 2N2

R. E. Camley *

Center for Magnetism and Magnetic Nanostructures

University of Colorado at Colorado Springs

Colorado Springs, CO 80933-7150

* Corresponding author

Abstract

Micron sized rectangular ferromagnetic bars have a variety of spin excitations, including a quasi-uniform mode, horizontal and vertical standing spin wave modes, and edge and corner modes. When driven by a strong microwave field, these modes differ from those found in the linear regime. For example, the resonance field or frequency becomes amplitude dependent. We study the nonlinear spin dynamics in such microstrips both experimentally and theoretically for a geometry where the static magnetic field is perpendicular to the plane of the sample. Experimentally it is found that, at a fixed microwave frequency, the resonance field for the uniform mode is significantly reduced as the microwave power is increased. In contrast, the resonance fields for the standing horizontal spin wave modes are only slightly reduced. This behavior is confirmed theoretically using micromagnetic calculations, and an intuitive explanation for this behavior is developed.

I. Introduction

The dynamic properties of ferromagnets and ferrimagnets have been studied for many years using ferromagnetic resonance (FMR) techniques. A particularly interesting feature of FMR is that it can provide detailed measurements of a complex nonlinear system by supplying sufficient power to drive the precession angle of the spins into the large amplitude regime.

Early observations of nonlinear effects in magnetic systems were demonstrated in Yittrium Iron Garnet (YIG), when it was discovered[1] that the resonance saturated at surprisingly low power. This behavior was subsequently explained by Suhl[2], and subsidiary absorptions were observed confirming the presence of Suhl's instabilities. An excellent summary of these early studies and related theory can be found in a review article by Patton[3]. Since that time there have been many studies on the nonlinear behavior in magnetic materials. For example, bright and dark solitons have been observed in feedback rings fabricated from YIG[4], and chaotic solitary spin wave pulses have also been produced.[5] Excellent summaries of nonlinear effects in ferromagnetic resonance studies of garnet materials are available.[6,7]

Until recently studies of nonlinear phenomena in magnetic systems were carried out in YIG, or in closely related materials. The reason is that the narrow linewidth of these samples allowed a large nonlinear response (mostly near resonance) at modest applied microwave power. Recently there have also been studies of nonlinear behavior in metals[8,9,10,11,12,13] This has become possible, in part, because in small-scale geometries one can obtain large microwave fields. There are also current driven experiments in

metallic systems where the effective damping is significantly reduced through the spin torque transfer effect.[14]

With the improvements of growth and patterning techniques, attention has turned to the dynamic magnetic behavior in micron and nanometer sized objects. For example, in small ferromagnetic bars, one observes a variety of excitations[15,16]. These include a quasi-uniform mode (often called the FMR mode because of its large absorption of energy), localized edge modes, and horizontal standing spin wave modes. The linear and nonlinear behavior of these modes is a field of active investigation.[17, 18, 19, 20]

The high quality of some new measuring techniques allows us to do measurements on the nonlinear behavior of both the FMR mode and the individual horizontal standing wave modes in a small micron-sized ferromagnetic bar. We consider the case where the magnetic field is applied perpendicular to the plane of the sample. We find that, at a fixed frequency, the resonance field of all the modes decreases as the microwave field is increased. However, there are substantial differences in the width and position of the resonance for the different modes, and in their position as a function of microwave power. We present both experimental and theoretical results in our examination, and show through a simple argument why the nonlinear behavior is different for the different modes.

II. Experiment

The experimental principle and setup configuration is described in detail in Ref [21,22] and illustrated in Fig 1. Essentially one has a ferromagnetic bar which is made of Permalloy ($Ni_{80}Fe_{20}$, Py) and which has a length of 300 microns, a width of 5-10 microns and a thickness of 100 nm deposited on a semi-insulating GaAs substrate. The

microwave fields are sent into the structure by a coplanar waveguide (CPW) fabricated by a metallic bilayer of Cu/Cr (200/10 nm) and the Py microstrip is situated underneath the short end of CPW. Between them a 200 nm SiO_2 layer is used for dc electrical isolation. Such vertical coupling architecture yields an in-plane microwave field as high as a few 10 mT inside the Py microstrip.

An external static magnetic field is applied nearly perpendicular to the plane of the bar at an angle of about 0.2^o with respect to the normal. A microwave signal as high as 25 dBm is sent into the waveguide and produces both an oscillating electric field and an oscillating magnetic field in the Py bar. As a result, a small dc voltage is induced along the length of the bar because of the ohmic coupling between the oscillating current due to microwave electric field and the oscillating resistance due to microwave magnetic field. The voltage shows peaks which correspond to the horizontal standing spin waves and the FMR mode[21]. The measurements were carried by the standard lock-in technique by 100% modulating the amplitude of microwave power with a 8.33 kHz square wave. The lock-in technique significantly enhances the signal/noise ratio, which enables us to detect a voltage signal weaker than 10 nV. This high sensitivity of the electrical detection enables us to see up to 6 quantized modes.

In Fig. 2 we present data showing the evolution of the voltage signal as a function of the power sent into the waveguide and the applied magnetic field for a microwave frequency of 4 GHz for a Py microstrip with a width of 5 μm. In Fig. 2a we see the induced voltage (symbols) measured as a function of field when the input power is 1 mW (0 dBm). This is a typical spectrum, with the FMR mode, A, showing the largest voltage and the standing modes (B, C, and D) having progressively smaller peaks. Our previous

study in the linear regime[21] has found that the resonant conditions of the horizontal standing spin waves (B, C, and D) are essentially determined by the dipole-dipole interactions, i.e, these modes have the nature of magnetostatic forward volume modes but with quantized wave vectors along the in-plane transversal direction of the microstrip. At the low power, all the peaks are symmetric about their resonance field which can be well fitted by the Lorentz line-shape (solid line).

In Fig. 2b, we show, using a color map, how this voltage spectrum changes as the input power is increased. At the fixed frequency of 4 GHz we see a series of vertical lines at low power. These lines show the resonant fields for the FMR mode, the intense line at the right hand side, and the different horizontal standing waves. As the power in the waveguide is increased the oscillating microwave field is increased and the lines bend to the left so that resonant (static) field is reduced. The largest shift is for the FMR mode; the horizontal standing spin wave modes have a smaller shift. We will present a simple explanation for this behavior in the next section. As a consequence of the difference in the shift, the horizontal standing spin wave modes merge into the FMR mode at higher microwave powers as clearly demonstrated in Fig. 2(b), where the FMR merges with mode B at about 40 mW. We note that color map also shows that the FMR peak (as seen in Fig 2a) becomes highly asymmetric, with the intensity sharply increasing on the low field side of the resonance and then decreasing with a broad tail on the high field side, which can be attributed to a so-called foldover FMR effect as detailed in the discussion in Ref. 22.

The foldover effect depends on the nonlinear nature of the spin system. At low power the voltage curve is symmetric about the resonance field but as the power

increases the position of the maximum shifts to lower fields by an amount that depends on the absorption amplitude. The voltage curve becomes asymmetric but with a single maximum. This behavior is characteristic of a driven nonlinear resonance[23]. At much higher power than used in these experiments, the voltage amplitude can become multi-valued at a given value of the field and exhibits foldover.

The features seen in Fig. 2 that the resonance fields for all modes shift downward as the microwave power is increased, and furthermore the largest shift is for the FMR mode, are generally applicable at all frequencies for all samples with different widths of 5-10 microns. Figure 3 presents a color map showing the dependence of the voltage signal on field and input power for different frequencies measured on a sample with a width of 7 μm. Similar trends are found as those in Fig. 2.

III. Micromagnetic Simulations

To obtain the key behavior of the nonlinear driven system, we use a very simple structure for the numerical calculation for the Py film as shown in Fig. 4. In this problem, we do not consider standing waves along the long axis nor through the thickness. The structure is divided into 128 cells in the x direction. This allows a good description of the longer wavelength standing waves which are seen in the experiment. We have done individual calculations with both a larger and smaller number of cells in the x direction; the results are essentially the same.

The dynamic micromagnetic calculation uses the Landau-Lifshitz (LL) equation to find the magnetization of each of the cells as it evolves through time. The LL equation is as follows:

$$\frac{\partial \vec{M}}{\partial t} = -|\gamma|(\vec{M}\times\vec{H}_{eff}) - |\gamma|\frac{\alpha}{M_s}(\vec{M}\times\vec{M}\times\vec{H}_{eff}) \quad (1)$$

where $\vec{M}$ is the magnetization of the cell and $\vec{H}_{eff}$ is the effective magnetic field present in the cell and is given by

$$\vec{H}_{eff} = \vec{H}_0 + \vec{H}_{ex} + \vec{H}_{dip} + h_d \cos(\omega t)\hat{y} + \vec{H}_A \quad (2)$$

$\vec{H}_0$ is the external static magnetic field, $\vec{H}_{ex}$ is the effective exchange field between nearest neighbor cells, $\vec{H}_{dip}$ includes the dipole fields created from all cells including the single cell's own demagnetizing field , and $h_d \cos(\omega t)\hat{y}$ is the driving field from the microwave field when it is present. The dipole field is calculated efficiently through a standard FFT method. The parameters for the calculation are as follows: the saturation magnetization is $\mu_0 M_s$ = 1.014 Tesla, the gyromagnetic ratio is 26.7 GHz/Tesla, the exchange constant is A = 1.3 x 10^{-11} J/m and the damping constant α = 0.01. The width of the Py bar is taken as 5 microns.

The coupled set of magnetic cells is driven with an oscillating field, h_d, at a given frequency. The oscillating field is directed along the y axis, but varies linearly in amplitude with x. (This allows us to pick up both odd and even modes in the results). To measure the response, we calculate the time-averaged power absorbed in a cell with dynamic magnetization $\vec{M}(t)$. This is given by

$$Average\ Abs\ Power = \frac{1}{T}\int_0^T \vec{h}_d(t) \bullet \frac{d\vec{M}(t)}{dt} dt \quad (3)$$

Here T is the oscillation period of the driving field, $\vec{M}(t)$ is the magnetization in a single cell and $\vec{h}_d(t)$ is the driving microwave field in the same cell. One then has to sum over

all cells in the magnetic structure to obtain the total absorbed power. In the nonlinear problem there are some additional considerations. First, as one scans over the values of the static magnetic field there will be some initial transients at each new field, and one must wait for these to die down before a calculation is made. Second, because the system is nonlinear, all the relevant behaviors will not be evident in a single period. One must, therefore, collect data over many periods in the hope of capturing all typical motions.

An example of the results is shown in Fig. 5. Here we plot the time-average absorption as a function of the applied field for oscillating driving fields, h_d, with different strengths. The frequency is fixed at 4.0 GHz allowing a comparison with Fig. 2. We see a series of peaks, with the largest one (the FMR peak) at the highest field value. The FMR peak is substantially larger than that of the standing wave modes, as is found in the experiment.

For a small driving field ($\mu_o h_d$ = 0.1 mT) we see well-defined, vertically oriented, peaks. As the driving field is increased, several changes occur: 1) The peaks shift to lower fields. The largest shift is for the FMR mode, with smaller shifts in the standing wave modes. 2) The peaks begin to lean over toward lower fields – the foldover effect. Again the effect is smaller for the standing wave modes. The FMR mode, in particular, shows a very broad peak, with the largest signal coming near a sharp low field edge. 3) The FMR mode and the first several standing wave modes seem to merge together at high power with a very extended tail on the high field side. All these features are in good agreement with the experimental results seen in Figs. 2 and 3.

Figure 6 shows a summary of the numerical results for the resonance field at a fixed frequency of 4 GHz and for different driving fields, h_d. One sees that the general

trends found in the experimental results of Fig. 2 are well reproduced in the theoretical calculations. In particular, one notes that at low microwave fields there is no shift in the resonance field. As the microwave amplitude is increased, the resonance fields shift down with the largest shift occurring for the FMR mode.

We can obtain a good physical understanding of this behavior through a simple argument relating to the precession angle. The resonance field for the perpendicular geometry is given by the simple expression

$$H_{res} = \omega / \gamma + M_z \qquad (4)$$

for an infinite slab. The finite dimensions of the bar will shift the resonance field to lower values but the effect is small and depends on the ratio of the thickness to the width. The usual argument for the power-dependence of the position of the FMR mode is as the power is increased, the precession angle increases, the z component of M decreases, the static demagnetizing field decreases, and thus the FMR field decreases. We note that a similar argument is also often invoked for the in-plane ferromagnetic resonance. Although it gives a reasonable qualitative understanding in some cases, the in-plane situation is more complex because of other modes degenerate with the FMR mode and the behavior of resonance field as a function of input power can even be nonmonotonic.[11]

The same considerations (an increase in precession angle leading to a decrease in the demagnetizing field and the resonance field) hold for the horizontal standing spin waves except for two features:

1) The amplitude of the standing spin waves is smaller than for the FMR as indicated in Fig 5. They are not driven as effectively as the FMR mode. This explains why the

standing modes do not see as much of a field shift as the power is increased. Their amplitude is lower, leading to a smaller reduction in M_z.

2) For the horizontal standing spin waves, the static demagnetizing field is not uniform. In the uniform mode, there is a nearly uniform distribution of surface magnetic charges causing a nearly uniform demagnetizing field as illustrated in Fig. 7a. For a standing mode with a half wavelength, as seen in Fig. 7b for example, we would have a nonuniform distribution of charges. Nonetheless, all the charges on one surface have the same sign even though there is a node in the middle of the film. Here all the magnetic surface charges on the top surface are positive and all of the charges on the lower surface would be negative. So, the demagnetizing field may not be uniform, but an increase in the precession amplitude will still cause a general decrease in surface charges and should lower the resonance field.

In the experiment, the oscillating field is produced by the ac current in the signal line. A simple estimation shows that one can expect a significant decrease in the amplitude of the microwave field across the width of the Permalloy sample. It is for this reason that we have used a nonuniform microwave field in the examples above. Nonetheless, it is interesting to see what would happen with a uniform microwave field. Fig. 8 presents the FMR absorption spectrum for such a situation. It is clear, that every other peak seen in Fig. 5 is now missing in Fig. 8. The reason for this similar is to that which explains the absorption of microwave energy by vertical standing spin wave modes. The uniform driving field is even about the midplane of the film – in this case the midplane along the length of the film. In contrast, with symmetric boundary conditions, standing modes which are odd cannot be excited by the uniform microwave field. In the

nonlinear limit however this may change. We note that the standing modes may hybridize with an edge mode to produce an asymmetry that allows energy absorption for the odd modes. Despite the differences in the two cases, the general trends found earlier – the reduction in the resonance field as the microwave power is increased – is clearly seen in Fig. 8 as it is in Fig. 5 and 6.

The results presented above considered the total power absorbed in the microstrip and were obtained using a simplified structure as discussed earlier. The advantage of this is that the numerical computations are significantly shorter. However, it is also helpful to calculate the distribution of power absorption across the width of the strip. These calculations required extensive computational resources and were obtained using the NIST software package known as OOMMF[24] after adapting the code to a parallel computer architecture. Smaller unit cells were investigated but the results did not change significantly. The results that follow were obtained using cells of size 300 x .3125 x .1 (μm). The saturation magnetization is $\mu_0 M_s$ =1.0 T, the gyromagnetic ratio is 26.7 GHz/T, the exchange constant is A = 1.4 x 10^{-11} J/m, and the damping constant is α = 0.04. In addition, the width of the Py bar is taken to be 10 microns. These parameter values differ slightly from those used in the calculations discussed above but the smaller value of M_s and the larger width also give excellent agreement with the experimental measurements.

Fig. 9 shows a detailed comparison of (a) the experimental photovoltage measurements and (b) the results obtained from our micromagnetic simulations for the mode amplitude m_y with a uniform microwave field. The shifts of the resonance frequencies with increasing microwave power (or amplitude of the driving field h_d) show excellent agreement. All modes shift downward in terms of the static field value and

approach one another as the amplitude of the driving field is increased. The A and B modes have merged by the time the driving field amplitude h_d has reached 3 mT. Just below this value where the two modes approach one another, their amplitudes increase indicating that the FMR mode is driving the B mode by means of a non-linear coupling. This feature is more evident in Fig. 10 which shows color maps of the spatial distribution of the standing wave amplitudes across the width of the bar as a function of the static field for driving fields of (a) 1 mT and (b) 3mT. Again a uniform microwave field is used and only symmetric modes are excited. At $\mu_0 h_d$ = 1 mT, the dominant amplitude is the FMR mode A and the standing wave modes B and C are clearly visible with smaller amplitudes. The horizontal standing wave modes have an odd number of amplitude peaks. At the higher field value of $\mu_0 h_d$ = 3 mT, the modes A and B have merged and the FMR mode has broadened significantly both in the static field and across the width. This may be expected since the B mode has more amplitude near the edges. In addition, the amplitude of the modes with 5 and 7 peaks have increased significantly as a result of the nonlinear coupling with the FMR mode.

Figure 11 shows a color map of the mode evolution with driving field amplitude for a strip of width 10 μm which can be compared with the experimental results for the 5 μm width sample in Fig 2b. The same qualitative features are found in both figures: a shift and broadening of the modes as the input power is increased and an increase in the amplitudes of the modes due to the non-linear coupling with the FMR mode.

IV. Summary

We have studied the nonlinear ferromagnetic dynamics of the uniform mode and the horizontal standing spin wave modes in a micron sized rectangular Permalloy bar. The magnetic field is applied perpendicular to the plane of the sample. Experimentally it is found that the resonance field for the uniform mode is significantly reduced as the microwave power is increased. In contrast, the resonance fields for the standing horizontal spin wave modes are only slightly reduced. Using a micromagnetic calculation for the power absorbed, we show the same general behavior theoretically. These results can be understood intuitively through a simple model. As the precession angle becomes larger, the demagnetizing field from the z component is reduced, which leads to a reduction in the resonance field. This is true for both the FMR mode and the standing spin wave modes, however the amplitude of the standing modes is smaller, leading to a smaller reduction in the resonance field. We also point out that the hybridization of the standing modes with an edge mode can change the absorption spectrum, particularly in the nonlinear limit.

Acknowledgments

The work of REC was supported by NSF Grant No. DMR 0907063. The work of CMH and BWS was supported by NSERC Grants. We also acknowledge the computing resources made available through Compute Canada.

Figure Captions:

Figure 1**:** (color online) Illustration of experimental geometry. (a) Schematic drawing of the sample structure, where a Py microstrip is underneath the short end of a coplanar waveguide (CPW) fabricated by metallic bilayer of Cu/Cr. Between them a SiO_2 layer is used for dc electrical isolation. (b) Top view micrograph of a device with Py strips underneath the short end of CPW between the ground (G) and signal (S) lines and the measurement circuitry.

Figure 2: (color online) (a) typical photovoltage curve as a function of magnetic field with an input signal at 4 GHz and an input power of 1 mW. Symbols are experimental data and the solid line is multi-Lorentzian fitting. The FMR mode is labeled A and the standing wave modes are B, C, and D. (b) Map of the voltage signal as a function of both the input power and applied magnetic field, where the voltage signal is normalized by the voltage at FMR for each power. The width of the sample is 5 μm.

Figure 3: (color online) Maps of the photovoltage signal as a function of the microwave power sent into the waveguide and the applied magnetic field for different frequencies. The width of the sample is 7 μm.

Figure 4: (color online) Illustration of the geometry used for the micromagnetic calculations. The structure is broken into 128 noncubic cells for the simulation. The applied field is canted at a small angle, 0.2^o , with respect to the vertical z axis.

Figure 5: Absorbed power as a function of static field for different values of the driving field obtained from the micromagnetic calculation. The frequency is set at 4 GHz. As the amplitude of the oscillating field is increased the peaks shift to lower field and develop a pronounced tail on the high field side. At very high driving fields several peaks merge together.

Figure 6: The influence of the microwave driving field on the resonance field as found in the micromagnetic calculation. As the driving field is increased the resonance field of all modes is shifted down, with the FMR mode experiencing the largest shift.

Figure 7: Schematic of the distribution of magnetic surface charges for the FMR mode and the first horizontal standing wave. The surface charges come from the vertical component of magnetization, so larger transverse components reduce the number of surface charges.

Figure 8: (color online) The FMR absorption spectrum for different values of the driving field. In contrast to Fig. 5, the microwave field is spatially uniform here. As a result, one sees absorption peaks from only half the modes. It is interesting to note that as the power is increased some of the missing modes begin to appear in the absorption spectrum.

Figure 9: (color online) (a) The experimental photovoltage in arbitrary units as a function of the static field at 4GHz for various input microwave powers. The FMR mode is labeled A and the standing wave modes are B and C. (b) The calculated values of the

mode amplitude m_y as a function of the static field at 4 GHz for various amplitudes of the microwave driving field h_d. The modes are labeled as in (a).

Figure 10: (color online) (a) Amplitude of standing wave modes as a function of position across the width and static field for a driving field of 1mT. The FMR mode is labeled as A and has the largest amplitude. Standing wave B is the next symmetric mode with 3 amplitude peaks and C has 5 peaks. (b) Same as above but with a driving field of 3 mT. The FMR mode has broadened asymmetrically and merged with the standing wave mode B.

Figure 11: (color online) Color map of the calculated mode amplitude integrated across the width as a function of the driving field and static field. The FMR mode is labeled A and the standing wave modes are labeled B and C.

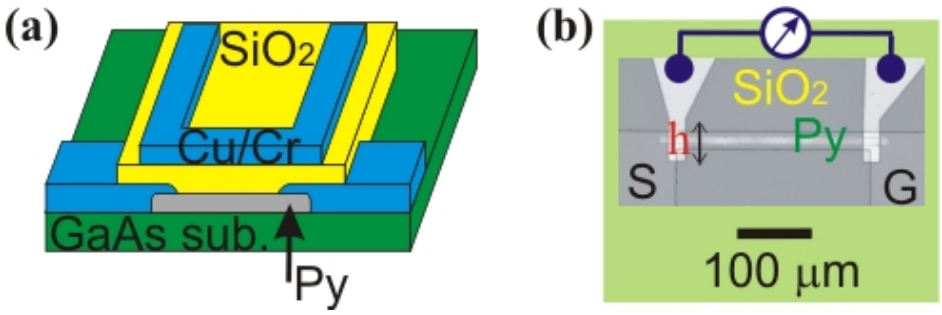

Fig. 1: (color online) Illustration of experimental geometry. (a) Schematic drawing of the sample structure, where a Py microstrip is underneath the short end of a coplanar waveguide (CPW) fabricated by metallic bilayer of Cu/Cr. Between the CPW and Py microstrip a SiO_2 layer is used for dc electrical isolation. (b) Top view micrograph of a device with Py strips underneath the short end of CPW between the ground (G) and signal (S) lines and the measurement circuitry.

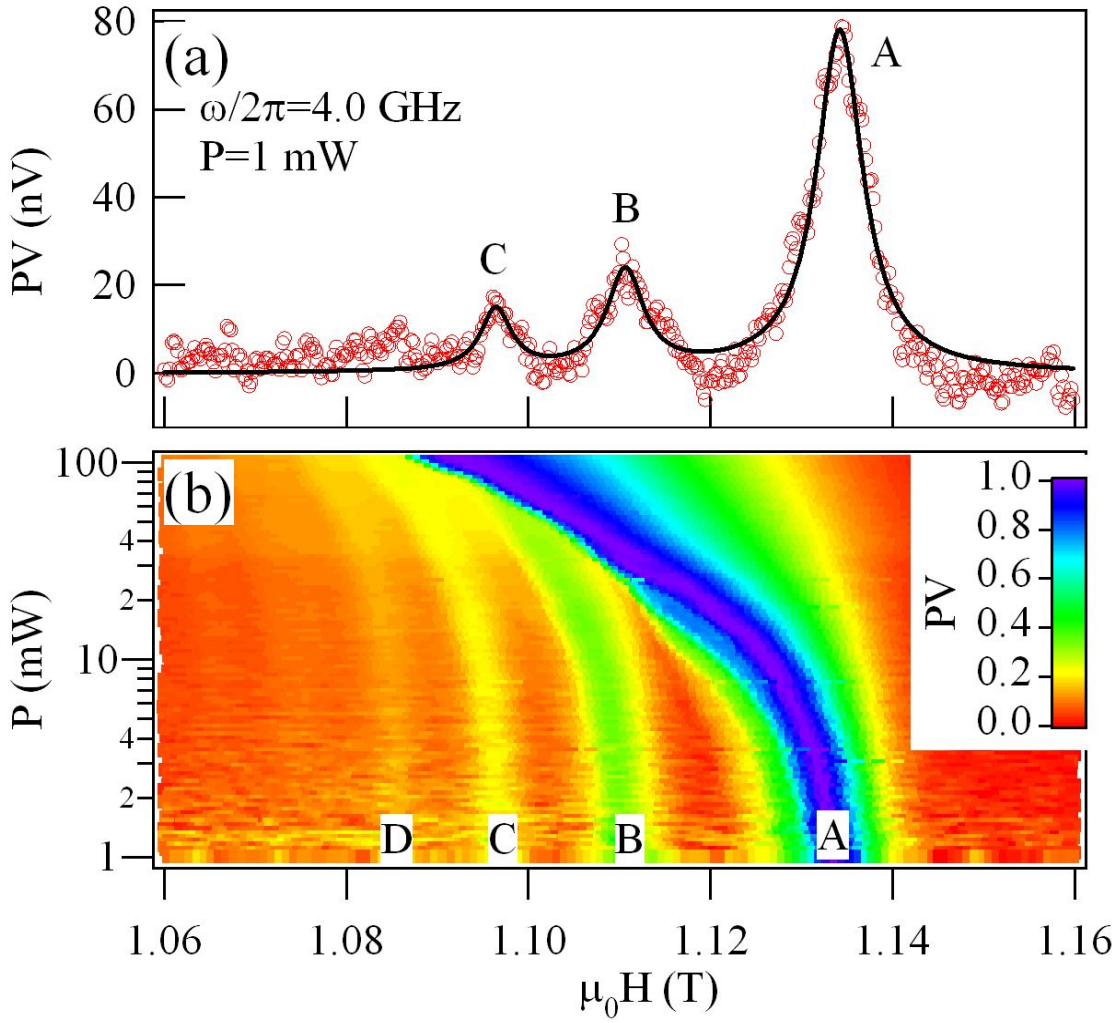

Figure 2: (color online) (a) typical photovoltage curve as a function of magnetic field with an input signal at 4 GHz and an input power of 1 mW. Symbols are experimental data and the solid line is multi-Lorentzian fitting. The FMR mode is labeled A and the standing wave modes are B, C, and D. (b) Map of the voltage signal as a function of both the input power and applied magnetic field, where the voltage signal is normalized by the voltage at FMR for each power. The width of the sample is 5 μm.

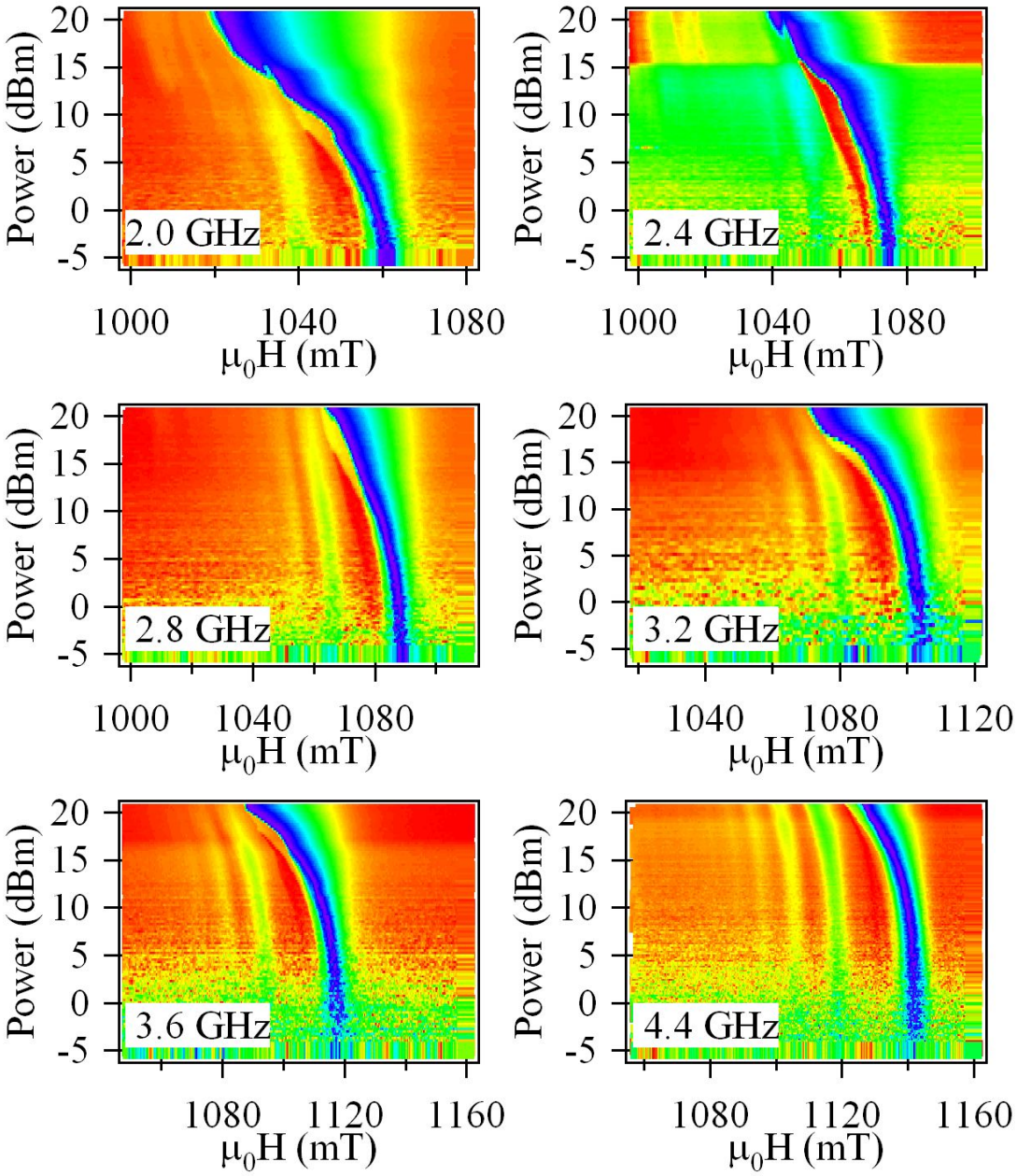

Figure 3 (color online) Maps of the voltage signal as a function of the power sent into the waveguide and the applied magnetic field for different frequencies. The width of the sample is 7 μm.

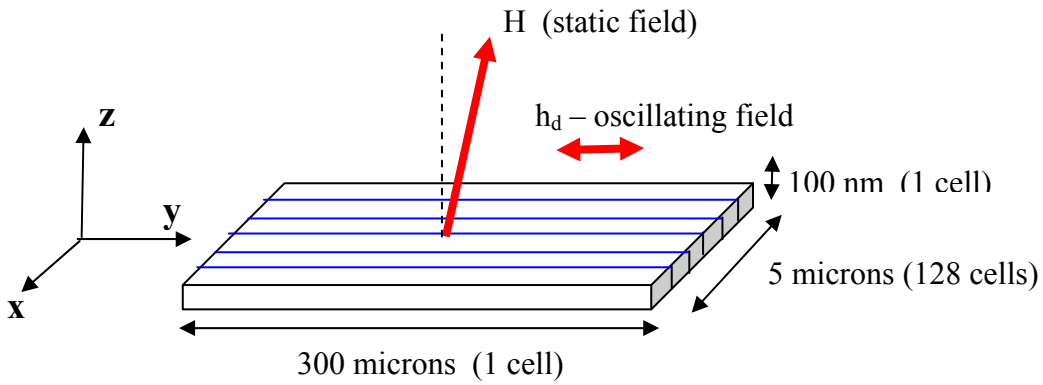

Figure 4: Illustration of the geometry used for the micromagnetic calculations. The structure is broken into 128 noncubic cells for the simulation. The applied field is canted at a small angle with respect to the vertical z axis.

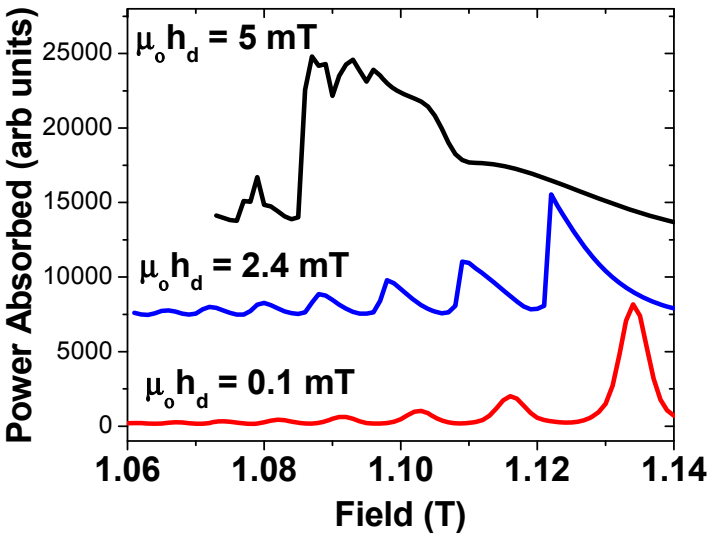

Figure 5: Absorbed power as a function of static field for different values of the driving field obtained from the micromagnetic calculation. The frequency is set at 4 GHz. As the amplitude of the oscillating field is increased the peaks shift to lower field and develop a pronounced tail on the high field side. At very high driving fields several peaks merge together.

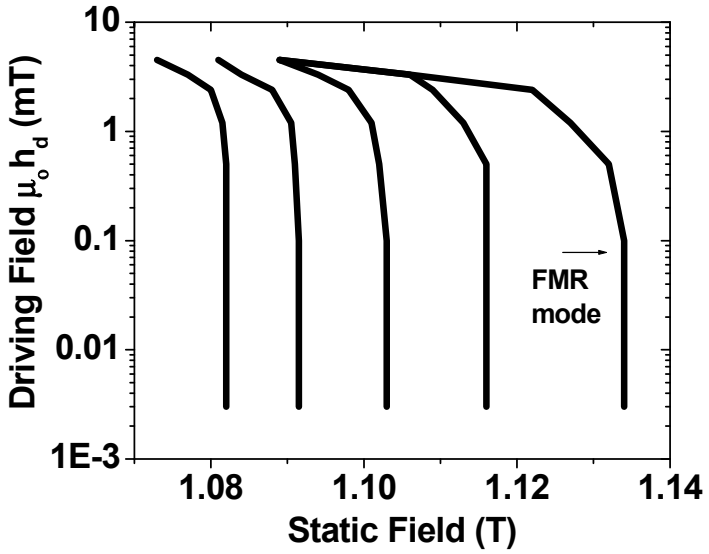

Figure 6: The influence of the microwave driving field on the resonance field as found in the micromagnetic calculation. As the driving field is increased the resonance field of all modes is shifted down, with the FMR mode experiencing the largest shift.

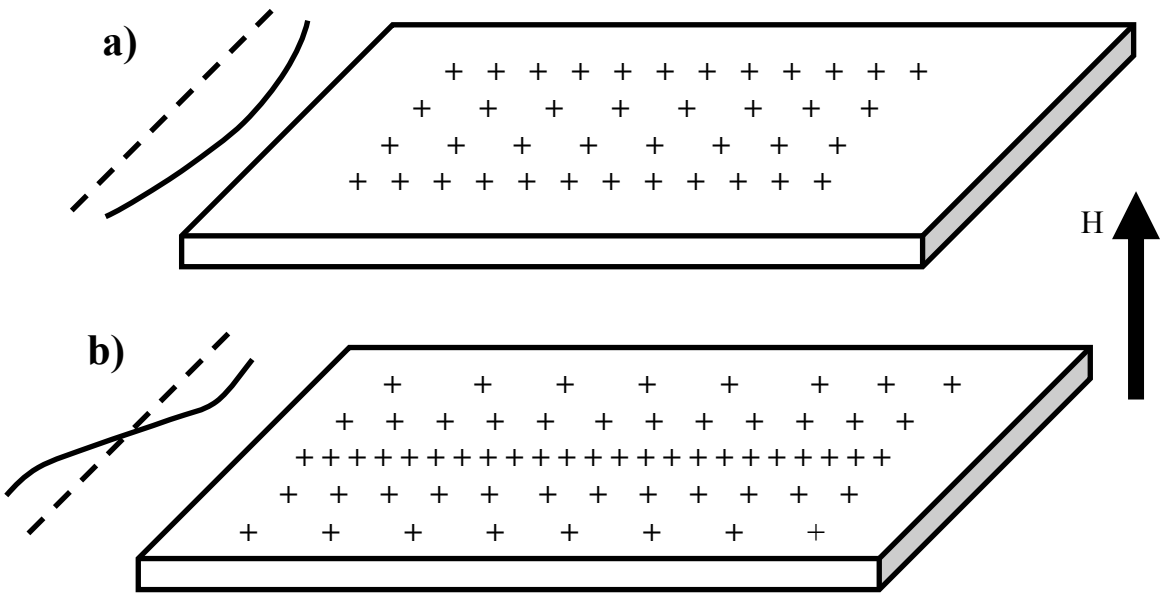

Figure 7: Schematic of the distribution of magnetic surface charges for the FMR mode and the first horizontal standing wave. The surface charges come from the vertical component of magnetization, so larger transverse components reduce the number of surface charges.

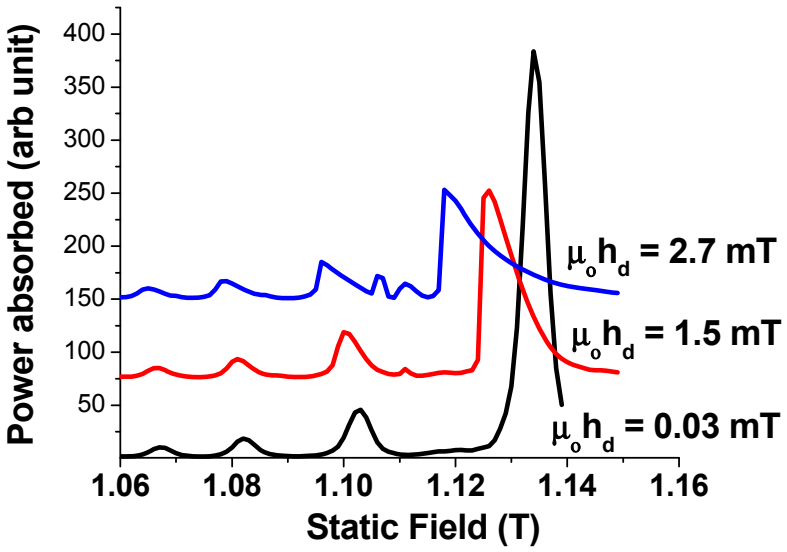

Figure 8: (color online) The FMR absorption spectrum for different values of the driving field. In contrast to Fig. 5, the microwave field is spatially uniform here. As a result, one sees absorption peaks from only half the modes. It is interesting to note that as the power is increased some of the missing modes begin to appear in the absorption spectrum.

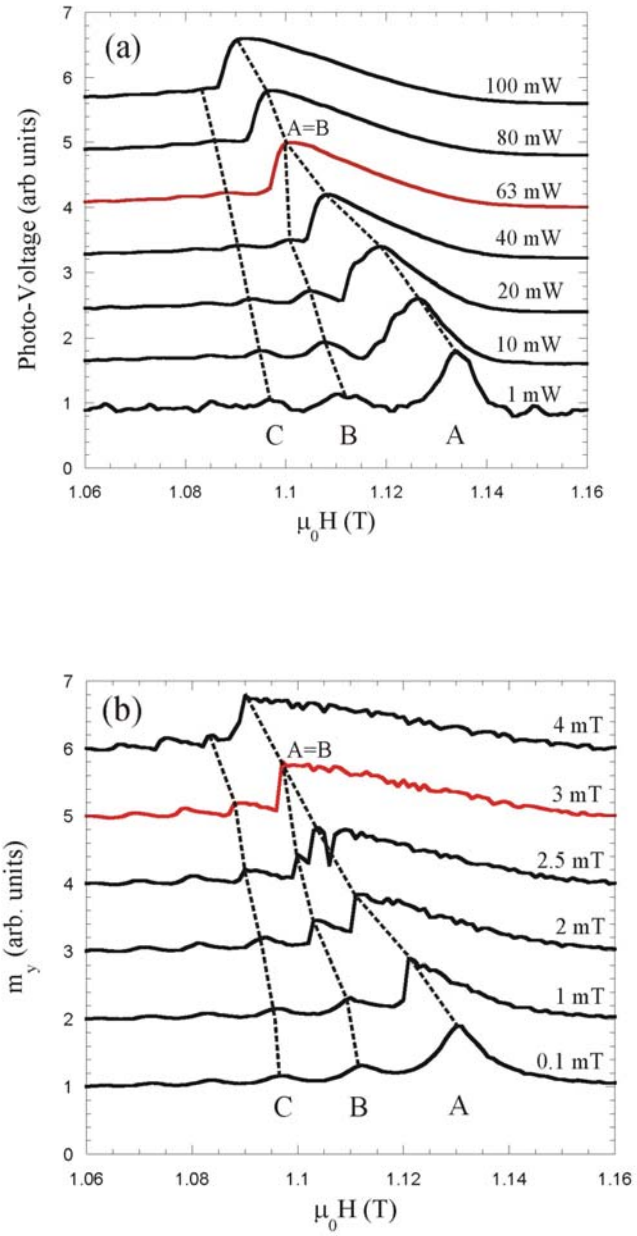

Figure 9: (color online) (a) The experimental photovoltage in arbitrary units as a function of the static field at 4GHz for various input microwave powers. The FMR mode is labeled A and the standing wave modes are B and C. (b) The calculated values of the mode amplitude m_y as a function of the static field at 4 GHz for various amplitudes of the microwave driving field $\mu_0 h_d$. The modes are labeled as in (a).

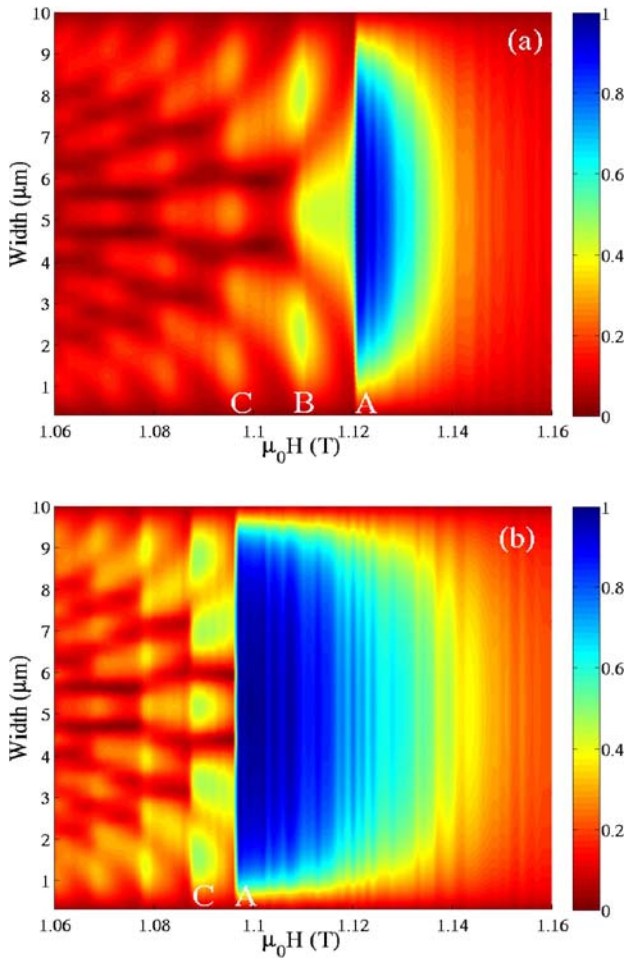

Figure 10: (color online) (a) Amplitude of standing wave modes as a function of position across the width and static field for a driving field of 1mT. The FMR mode is labeled as A and has the largest amplitude. Standing wave B is the next symmetric mode with 3 amplitude peaks and C has 5 peaks. (b) Same as above but with a driving field of 3 mT. The FMR mode has broadened asymmetrically and merged with the standing wave mode B. The intensity of mode C has increased susbstantially.

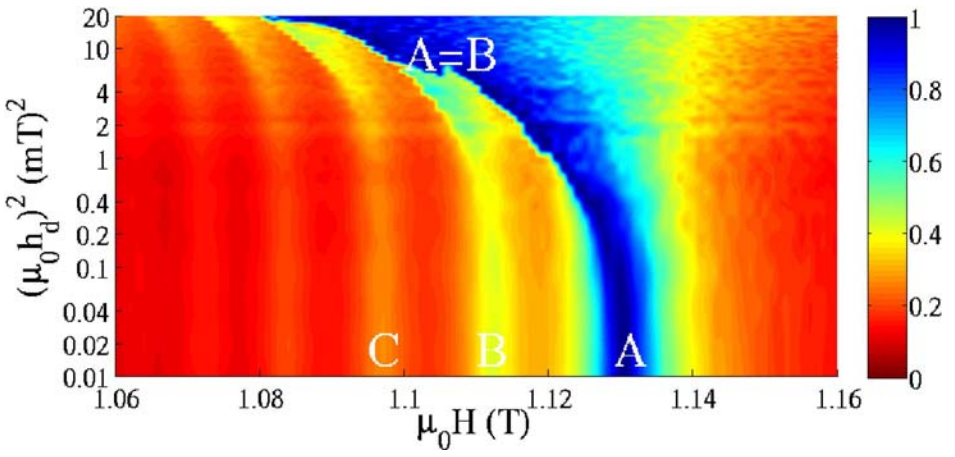

Figure 11: (color online) Color map of the calculated mode amplitude integrated across the width as a function of the driving field and static field. The FMR mode is labeled A and the standing wave modes are labeled B and C.

References

[1] N. Bloembergen and R. W. Damon, Phys. Rev. **85**, 699 (1952)

[2] H. Suhl, Phys. Rev. 101, 1437 (1956); J. Phys. Chem. Solids **1**, 209 (1957)

[3] Carl E. Patton, Phys. Rep. **103**, 251 (1984)

[4] B. A. Kalinikos, N. G. Kovshikov, and C. E. Patton, Phys. Rev. Lett. **80**, 4301 (1998)

[5] M. Wu, B. A. Kalinikos, and C. E. Patton, Phys. Rev. Lett. **95**, 237202 (2005)

[6] Nonlinear Phenomena and Chaos in Magnetic Materials, edited by P. E. Wigen (World Scientific, Singapore, 1994)

[7] S. O. Demokritov, B. Hillebrands, and A. Slavin, Phys. Rep. **348**, 441 (2001)

[8] V. E. Demidov, U.-H. Hansen, and S. O. Demokritov, Phys. Rev. Lett. **98**, 157203 (2007)

[9] H. M. Olson, P. Krivosik, K. Srinivasan, and C. E. Patton, J. Appl. Phys. **102**, 023904 (2007)

[10] M. Yan, P. Vavassori, G. Leaf, F. Y. Fradin, and M. Grimsditch, J. Magn. Magn. Mater. **320**, 1909 (2008)

[11] Y. Khivintsev, B. Kuanr, T. J. Fal, M. Haftel, R. E. Camley, Z. Celinski, and D. L. Mills, Physical Review B **81** 054436 (2010)

[12] Yuri Khivintsev, J. Marsh, V. Zagorodnii, I Harward I, J. Lovejoy , P Krivosik, R. E. Camley and Z. Celinski, Appl. Phys. Lett. **98**, 042505 (2011)

[13] Henning Ulrichs,Vladislav E. Demidov, Sergej O. Demokritov, Sergei Urazhdin, Phys. Rev. B **84**, 094401 (2011)

[14] C. T. Boone, J. A. Katine, J. R. Childress, V. Tiberkevich, A. Slavin, J. Zhu, X. Cheng, and I. N. Krivorotov, Phys. Rev. Lett. **103**, 167601 (2009)

[15] K. Y. Guslienko, S. O. Demokritov, B. Hillebrands, and A. N. Slavin, Phys. Rev. B **66** 132402 (2002)

[16] Marcos Grimsditch, Gary K. Leaf, Hans G. Kaper, Dmitry A. Karpeev, and Robert E. Camley, Phys. Rev. B **69,** 174428 (2004)

[17] R. D. McMichael and M. D. Stiles, J. Appl. Phys. **97**, 10J901 (2005)

[18] V. E. Demidov, M. Buchmeier, K. Rott, P. Krzysteczko, J. Münchenberger, G. Reiss, and S. O. Demokritov, Phys. Rev. Lett., **104**, 217203 (2010)

[19] Vladislav E. Demidov, Ulf-Hendrik Hansen, and Sergej O. Demokritov, Phys. Rev. Lett., **98**, 157203 (2007)

[20] V. S. Tiberkevich, Joo-Von Kim and A. N. Slavin , Phys.Rev. B **78** , 092401 (2008)

[21] Y. S. Gui, N. Mecking, X. Zhou, G. Williams, and C.-M. Hu, Phys. Rev. Lett., **98,** 107602 (2007); Y. S. Gui, N. Mecking, and C. -M. Hu, Phys. Rev. Lett. **98**, 217603 (2007)

[22] Y. S. Gui, A. Wirthmann, N. Mecking, and C.-M. Hu, Phys. Rev. B **80**, (R)060402 (2009); Y. S. Gui, A. Wirthmann, and C.-M. Hu, Phys. Rev. B **80**, 184422 (2009)

[23] L. D. Landau and E. M. Lifshitz, *Mechanics*, 2nd ed. Pergamon Press, Oxford, 1969.

[24] M. J. Donahue and D. G. Porter, National Institute of Standards and Technology, Interagency Report No. NISTIR6376, (1999)